Nonlinear dynamic analysis and control synthesis for the Swinging Omnidirectional (SWINGO) Wave Energy Converter

Available online at www.sciencedirect.com

ScienceDirect

IFAC Papers Online CONFERENCE PAPER ARCHIVE

IFAC PapersOnLine 56-2 (2023) 11723–11728

Nonlinear dynamic analysis and control synthesis for the Swinging Omnidirectional (SWINGO) Wave Energy Converter.

Fabio Carapellese [1] **, Bruno Paduano, Edoardo Pasta, Guglielmo Papini, Nicolás Faedo, and Giuliana Mattiazzo**

Marine Offshore Renewable Energy Lab., Department of Mechanical and Aerospace Engineering, Politecnico di Torino, 10129 Turin, Italy

Abstract: We introduce, in this paper, an analysis of the dynamics of the Swinging Omnidirectional (SWINGO) wave energy converter. Such a device is an inertial reacting Wave Energy Converter (WEC), that exploits the dynamics of a gyropendulum mechanism which, being excited by the wave-induced whirling motion (*i.e.* coupling between pitch and roll on a floater), can successively activate an electric generator connected to the grid. In particular, we apply the harmonic balance method, tuned to the system fundamental harmonic, to identify the effect of nonlinearities on the SWINGO dynamics and their impact on energy production. Furthermore, we present the so-called van der Pol plane to assess the stability properties of the system. The SWINGO model is derived via a Lagrangian approach formulated with respect to quasi-coordinates. We demonstrate that multi-stability behaviour can be found for this nonlinear system, completely absent in its associated linearisation. Finally, we synthesise so-called 'passive' (*i.e.* proportional) energy-maximising controllers by leveraging the Harmonic Balance (HB) procedure, providing control parameters which are effectively tuned by exploiting the presented nonlinear description of SWINGO.

Keywords: Wave energy converters, Nonlinear Modelling, Harmonic Balance

1. INTRODUCTION

Ocean wave energy is an untapped resource, with 10 TW of energy available worldwide (Gunn and Stock-Williams, 2012). Nevertheless, extraction of the wave resource presents problems in terms of maintenance, cost of energy, and technology limitations due to the wide-banded nature of ocean waves.

Most of the devices introduced in the literature are analysed in the linear domain, often driven by the motivation of keeping models simple for optimization and real-time control purposes. In fact, the design of wave energy converters (WECs) involves an optimization process which aims at lowering the associated cost of energy and maximising the amount of energy produced. The latter can be further optimised through the application of suitable control technology capable of 'expanding' the operating frequency range of WEC systems, which naturally have a narrow operating frequency band.

Although the use of linear models can be seen as a valid procedure within a first design stage, it may become an imprecise approximation for a full scale device implementation, since we recall that, in the wave energy research field, the infinitesimal motion assumptions, used to compute the system linearised model, are violated by the controller itself, which often moves the system away from its equilibrium position, to enhance the motion and effectively maximise energy extraction (Windt et al., 2021).

Generally, offshore WEC systems, which aim to harvest wave energy from a rotational degree-of-freedom (DoF), make use of a floater as an intermediate system to transmit the wave motion to an encapsulated inertial mass, *e.g.* pendulum (see (Gioia et al., 2022)), gyroscope (see (Carapellese et al., 2022a)), or sliding mass rigidly connected to an electric generator. Recently, we have introduced a newly-developed concept called *Swinging Omni-directional* (SWINGO) WEC in (Carapellese et al., 2023), designed for being a multidirectional device. On the basis of a more realistic wave representation, which includes the so-called spreading phenomenon, SWINGO is parametrically excited by pitch and roll motion of the floater, having a rich dynamical behaviour. Such nonlinear effects are not captured by a linearised model, providing inconsistent controller parametrisations.

We provide, in this paper, a detailed dynamical analysis for the SWINGO system, including the derivation of the optimal passive control parameters considering a comprehensive nonlinear description. In particular, we compute the nonlinear equations characterising the WEC system by using a Lagrangian approach defined for quasi-coordinates, and adopt a harmonic balance (HB) method to analyse the resulting nonlinear behaviour. In particular, we produce both the so-called amplitude-frequency curves (AFC), and the multi-stability curve for the corresponding SWINGO dynamics. We demonstrate that the SWINGO system can present dynamic behaviour totally neglected by its corresponding linearisation, including *e.g.* multi-stability. Therefore, based on the analysis of the system response

[1] Corresponding author - e-mail: *fabio.carapellese@polito.it.*

10.1016/j.ifacol.2023.10.540

through the van der Pol plane, the stability of each solution is analysed, to avoid driving the system through an unstable oscillation (especially under controlled conditions).

The reminder of this paper is organised as follows. Section 2 presents a derivation of the nonlinear SWINGO model, including a brief theoretical background on the HB procedure. Section 3 provides a control synthesis based upon HB to define the optimal passive control parameter for the nonlinear system, while Section 4 presents a dynamical analysis of the SWINGO system, with a particular focus on the system stability properties arising from different control settings. Finally, the main conclusions of this study are highlighted in Section 5.

2. SWINGO MODEL

The SWINGO device is composed of an innovative gyropendulum mechanism, mounted inside a floating hull, as in Figure 1. The gyropendulum mechanism is introduced in Meirovitch (1970), and adapted for wave energy applications in *e.g.* (Carapellese et al., 2023). It is a gyroscopic system, in which the flywheel mass m_f is essentially mounted at a distance l_f from the precession axis, as shown in Figure 1. The floater pitch motion 'activates' the mechanical system, which hence oscillates, according to an angle $\varepsilon : t \mapsto \varepsilon(t)$, due to the forces of the incoming wave field. Note that, it is well-known (see *e.g.* (Meirovitch, 1970)) that a gyroscopic system is parametrically excited if it is induced to rotate in the plane parallel to the floater deck. Such gyroscopic motion is then converted into electrical energy by means of a dedicated power take-off (PTO) actuator system.

For the subsequent analysis, we focus on the system response defined in terms of the vector $\gamma(t) = [\theta(t)\ \delta(t)]$, where $\theta : t \mapsto \theta(t) \in \mathbb{R}$ and $\delta : t \mapsto \delta(t) \in \mathbb{R}$ denote the floater roll and pitch rotation, respectively. We focus on an 'intermediate' condition to study the device property in hybrid mode, *i.e.* when the roll and pitch are considered.

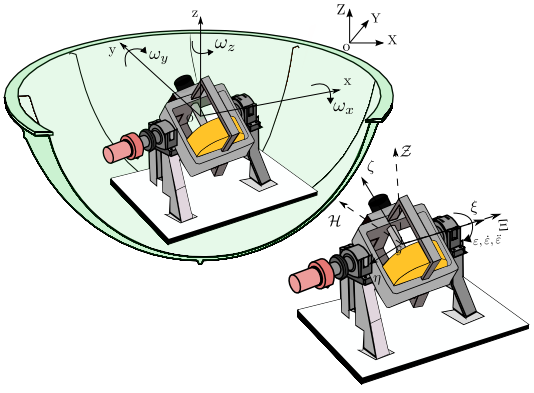

Fig. 1. Schematic representation of the SWINGO device.

2.1 Reference frame and kinematics definition

We derive, in this section, the fundamental nonlinear mathematical model describing the dynamics of the SWINGO device. Relative motion between bodies is involved during operating conditions, and hence we introduce hereafter a suitable set of reference frames:

- $\mathcal{R}(OXYZ)$ is the inertial reference frame,
- $\mathcal{R}(\mathcal{O}'\text{xyz})$ is the hull fixed reference frame, with the x-axis parallel to the ξ-axis and origin $\mathcal{O}'$ placed in the WEC center of gravity (CoG),
- $\mathcal{R}(\mathcal{G}\Xi\mathcal{H}\mathcal{Z})$ is the hull-fixed reference frame with the origin $\mathcal{G}$ on the gyropendulum precession axis, and
- $\mathcal{R}(\mathcal{G}\xi\eta\zeta)$ is the gimbal-fixed reference frame.

With the definition of the system reference frames above, we derive the full nonlinear equation of motion of the mechanism in terms of *quasi-coordinates* (see *e.g.* (Genta, 2009)), to transpose the floater-referred generalised coordinates γ on the gyropendulum-fixed reference frame, *i.e.* $\mathcal{R}(\mathcal{G}\xi\eta\zeta)$. We state the vector of quasi-coodinates $\Omega_f : t \mapsto \Omega_f(t) \in \mathbb{R}^3$, with $\Omega_f(t) = [\omega_\xi(t)\, \omega_\eta(t)\, \omega_\zeta(t)]^\mathsf{T}$ defined in $\mathcal{R}(\mathcal{G}\xi\eta\zeta)$ as follows,

$$\Omega_f = R(\varepsilon, \hat{\xi})^\mathsf{T} D \dot{\Phi} = J \dot{\Phi}, \tag{1}$$

where $R(\varepsilon, \hat{\xi})$ denotes the rotation matrix of angle ε, with respect to a unit vector $\hat{\xi}$ defined on the ξ-axis, and D is the inverse of the analytical Jacobian matrix as defined in (Siciliano et al., 2009). Moreover, $\dot{\Phi}(t) = [\dot{\gamma}(t)\, \dot{\psi}(t)]^\mathsf{T}$, where ψ is the floater yaw rotation, which is considered to be zero within this study. Therefore, the total velocity $\Omega_g : t \mapsto \Omega_g(t) \in \mathbb{R}^3$, with $\Omega_g(t) = [\Omega_\xi(t)\, \Omega_\eta(t)\, \Omega_\zeta(t)]^\mathsf{T}$ links the mapped floater velocity on $\mathcal{R}(\mathcal{G}\xi\eta\zeta)$, and the proper velocity of the gyropendulum $\dot{\varepsilon}$ is defined as,

$$\Omega_g = \begin{bmatrix} R(\varepsilon, \hat{\xi})^\mathsf{T} D & \tilde{I} \end{bmatrix} \begin{bmatrix} \dot{\Phi} \\ \dot{\varepsilon} \end{bmatrix}, \tag{2}$$

where $\tilde{I} = [1\ 0\ 0]^\mathsf{T}$. Finally, we define the total flywheel velocity $[\Omega_{\xi'}\, \Omega_{\eta'}\, \Omega_{\zeta'}]^\mathsf{T}$ as follows

$$\Omega_{\xi'} = \Omega_\xi, \qquad \Omega_{\eta'} = \Omega_\eta, \qquad \Omega_{\zeta'} = \Omega_\zeta + \dot{\varphi}, \tag{3}$$

where $\dot{\varphi}$ is the proper flywheel speed, considered constant during operating conditions, and set according to the wave direction. Note that, when $\dot{\varphi}$ is null, the gyropendulum behaves as a pendulum, which is the optimal condition when the wave direction is parallel to the y-axis. In contrast, when the waves move parallel to the x-axis, $\dot{\varphi}$ is set to a value different from zero, to activate the gyroscopic effect and exploit the coupling between the flywheel speed $\dot{\varphi}$, and the floater angular velocity with respect to the y-axis, *i.e.* $\dot{\delta}$.

2.2 Lagrange approach for quasi-coordinates

With the kinematics description of the gyropendulum system, presented in (1)-(2), we derive the vector of forces $T_{gp}(t) = [T_\xi(t)\ T_\eta(t)\ T_\zeta(t)]^\mathsf{T} \in \mathbb{R}^3$ acting on the gyropendulum, transmitted to the floater through the set of radial bearings that constraint the gyropendulum to the system. The equation of motion for the SWINGO system, by means of the Lagrange equations in terms of Ω_g, can be expressed as follows

$$\frac{d}{dt}\left(\frac{\partial \mathcal{T}}{\partial \Omega_g}\right) + \tilde{\omega}\frac{\partial \mathcal{T}}{\partial \Omega_g} + J^{-\mathsf{T}}\frac{\partial \mathcal{U}}{\partial \Phi} = T_{gp} \tag{4}$$

where $\mathcal{T}(\Omega_g) \in \mathbb{R}$ and $\mathcal{U}(\Phi) \in \mathbb{R}$ are the system kinetic and potential energy, respectively, and $\tilde{\omega}$ is the skew-symmetric matrix associated to Ω_g. Note that, the equation presented in (4) does not introduce the term related to the linear velocity of the floater, resulting in a modified version of the equation introduced in (Meirovitch, 1970). Finally,

the equation of motion defined in quasi-coordinates with respect to $\mathcal{R}(\mathcal{G}\xi\eta\zeta)$ is stated as follows:

$$\begin{bmatrix} I_\xi & 0 & 0 \\ 0 & I_\eta & 0 \\ 0 & 0 & I_\zeta \end{bmatrix} \begin{bmatrix} \dot{\omega_\xi} \\ \dot{\omega_\eta} \\ \dot{\omega_\zeta} \end{bmatrix} + \begin{bmatrix} 0 & I_\zeta\omega_\zeta + J\dot{\varphi} & -I_\eta\omega_\eta \\ I_\zeta\omega_\zeta - J\dot{\varphi} & 0 & I_\xi\omega_\xi \\ I_\eta\omega_\eta & -I_\xi\omega_\xi & 0 \end{bmatrix} \begin{bmatrix} \omega_\xi \\ \omega_\eta \\ \omega_\zeta \end{bmatrix} + \\ + \begin{bmatrix} 0 & 0 & 0 \\ 0 & 1 & 0 \\ 0 & 0 & 1 \end{bmatrix} \left(J^{-\mathsf{T}} \begin{bmatrix} \frac{\partial \mathcal{U}}{\partial \theta} \\ \frac{\partial \mathcal{U}}{\partial \delta} \\ \frac{\partial \mathcal{U}}{\partial \psi} \end{bmatrix} \right) + \begin{bmatrix} \frac{\partial \mathcal{U}}{\partial \varepsilon} \\ 0 \\ 0 \end{bmatrix} = T_{gp}, \tag{5}$$

where the corresponding inertia matrix of the gimbal, and flywheel system with respect to their CoG, $\{I_s, I_f\} \subset \mathbb{R}^{3\times3}$, are, respectively,

$$I_s = \text{diag}(I_{s,x}, I_{s,y}, I_{s,z}), \quad I_f = \text{diag}(I_{f,x}, I_{f,y}, I_{f,z}). \tag{6}$$

We define the inertial element introduced in (5) as follows,

$$\begin{aligned} I_\xi &= I_{s,x} + I_{f,x} + m_f l_f^2, \\ I_\eta &= I_{s,y} + I_{f,y} + m_f l_f^2, \\ I_\zeta &= I_{s,z} + I_{f,z}. \end{aligned} \tag{7}$$

We recall that T_ξ is null when the device is in non-operating conditions, and equal to T_{PTO} when effectively in energy extraction mode. In particular, we define the PTO (control) torque in terms of the following (passive) parametric expression:

$$T_{\text{PTO}} = -c_{\text{PTO}}\dot{\varepsilon}, \tag{8}$$

where $c_{\text{PTO}} \in \mathbb{R}^+$ is the (PTO) control parameter, adjusted to maximise energy conversion according to the frequency of the wave excitation force. As a further step, we transpose the derived reaction forces to the floater frame $\mathcal{R}(\mathcal{O}'\text{xyz})$, and we introduce the vector $T_f = [T_x\ T_y\ T_z]^\mathsf{T}$, derived as

$$T_f = R(\varepsilon, \hat{\xi})T_{gp}. \tag{9}$$

With the definitions provided up until this point, the nonlinear equation, which fully describes the mechanical interaction between the gyropendulum and the floater expressed in generalised coordinates, can be written as follows [2]

$$\begin{bmatrix} I_\xi & 0 & I_\xi \\ 0 & I_{y,i} & 0 \\ I_\xi & 0 & I_\xi \end{bmatrix} \begin{bmatrix} \ddot{\theta} \\ \ddot{\delta} \\ \ddot{\varepsilon} \end{bmatrix} = \begin{bmatrix} T_x \\ T_y \\ T_\xi + T_{\text{PTO}} \end{bmatrix} + \begin{bmatrix} 0 \\ 2I_{y,i}(s_\varepsilon c_\theta + c_\varepsilon s_\theta)\dot{\delta}\dot{\varepsilon} \\ 0 \end{bmatrix} \tag{10}$$

where $T_x = T_\xi$ and the inertia terms $I_{y,i}$ in (10) computed from the following equation

$$\begin{bmatrix} I_{x,i} & 0 & 0 \\ 0 & I_{y,i} & 0 \\ 0 & 0 & I_{z,i} \end{bmatrix} = R(\varepsilon, \hat{\xi}) \begin{bmatrix} I_\xi & 0 & 0 \\ 0 & I_\eta & 0 \\ 0 & 0 & I_\zeta \end{bmatrix} R(\varepsilon, \hat{\xi})^\mathsf{T} D. \tag{11}$$

2.3 Hydrodynamic model

With the assumption that the fluid is inviscid and incompressible, and the fluid flow is irrotational, the so-called *linear potential flow theory* (Falnes, 2002) provides an approximation of the fluid-structure interaction through a time-domain system of Volterra equations, written as

$$\Sigma : \left\{ I_h\ddot{\gamma} = T_w + T_h + T_r + T_{reac}, \right. \tag{12}$$

where $I_h \in \mathbb{R}^{2\times2}$ is the diagonal inertia matrix of the SWINGO device, and $T_{reac} = [T_x, T_y]^\mathsf{T}$ is the vector of reaction forces defined in the Section 2.2. $T_w = [T_{w_\theta}, T_{w_\delta}]^\mathsf{T} : \mathbb{R}^+ \to \mathbb{R}^2$ defines the (uncontrollable) wave excitation torque, $T_r : \mathbb{R}^+ \to \mathbb{R}^2$ is the so-called radiation torque vector, and $T_h : \mathbb{R}^+ \to \mathbb{R}^2$ describes the hydrostatic restoring torque acting on the floater. Such a force is defined proportional to the device (pitch) motion, and can be hence written as $T_h = [T_{h_\theta}, T_{h_\delta}]^\mathsf{T} = -S_h\gamma$, where $S_h \in \mathbb{R}^{2\times2}$ is the so-called hydrostatic stiffness coefficient. Note that, in this study, we are considering an incident angle $\alpha = 45^o$, and then the wave excitation forces on roll and pitch axes with respect to $\mathcal{R}(\mathcal{O}'\text{xyz})$ have the same amplitude, given the floater symmetry. Moreover, the radiation force is modelled using the well-known Cummins' equation, *i.e.*

$$T_r(t) = \begin{bmatrix} T_{r_\theta}(t) \\ T_{r_\delta}(t) \end{bmatrix} = -\left(m^\infty\ddot{\gamma}(t) + \int_{\mathbb{R}^+} h_r(t-\tau)\dot{\gamma}(\tau)\text{d}\tau \right), \tag{13}$$

where the first term in the summation, proportional to the device acceleration in pitch, corresponds to an inertial increase due to the water displaced when the body moves, while the second term corresponds with the dissipative force, proportional to the body velocity. In particular, the matrix $m^\infty \in \mathbb{R}^{2\times2}$ represents the so-called added-mass at infinite frequency, given by the relation $m^\infty = \lim_{\omega\to+\infty} A_r(\omega)$, where $A_r(\omega)$ is the so-called frequency-dependent added-mass coefficient (see (Falnes, 2002)).

2.4 Coupled mechanical-hydrodynamic model

Within this section, we provide the coupled mechanical-hydrodynamic model σ, by considering the inherent mechanical coupling between the gyropendulum mechanism and the floater, and the hydrodynamic (pitch and roll) motion of the device activated by the wave input torque. Therefore, by defining the hydrostatic stiffness matrix S_h and added mass m^∞ as follows

$$I_h = \begin{bmatrix} I_{h_\theta} & 0 \\ 0 & I_{h_\delta} \end{bmatrix}, S_h = \begin{bmatrix} S_{h_\theta} & 0 \\ 0 & S_{h_\delta} \end{bmatrix}, m^\infty = \begin{bmatrix} m_\theta^\infty & 0 \\ 0 & m_\delta^\infty \end{bmatrix}, \tag{14}$$

the nonlinear model σ of the SWINGO device can be expressed, in compact form, as

$$\begin{bmatrix} I_{h_\theta} + I_\xi + m_\theta^\infty & 0 & I_\xi \\ 0 & I_{h_\delta} + I_{y,i} + m_\delta^\infty & 0 \\ I_\xi & 0 & I_\xi \end{bmatrix} \begin{bmatrix} \ddot{\theta} \\ \ddot{\delta} \\ \ddot{\varepsilon} \end{bmatrix} = \begin{bmatrix} T_{w_\theta} + T_{h_\theta} + T_{r_\theta} + T_x \\ T_{w_\delta} + T_{h_\delta} + T_{r_\delta} + T_y \\ T_\xi + T_{\text{PTO}} \end{bmatrix}. \tag{15}$$

For the sake of completeness, we provide a derivation of the Jacobian linearisation of equation (15) for the SWINGO device as a 'reference' (i.e. benchmark) case model for the analysis performed in Section 3. The linearisation procedure is performed under the assumption of infinitesimally small rotation about the equilibrium position $(\theta, \delta, \varepsilon) = (0,0,0)$, hence the associated linearised system σ_l is:

$$\begin{bmatrix} I_{h_\theta} + I_\xi + m_\theta^\infty & 0 & I_\xi \\ 0 & I_{h_\delta} + I_\eta + m_\delta^\infty & 0 \\ I_\xi & 0 & I_\xi \end{bmatrix} \begin{bmatrix} \ddot{\theta} \\ \ddot{\delta} \\ \ddot{\varepsilon} \end{bmatrix} = \begin{bmatrix} T_{w_\theta} + T_{h_\theta} + T_{r_\theta} - J\varphi\dot{\delta} - m_f l_f g(\theta + \varepsilon) \\ T_{w_\delta} + T_{h_\delta} + T_{r_\delta} + J\varphi(\dot{\theta} + \dot{\varepsilon}) - m_f l_f g\delta \\ T_{\text{PTO}} - J\varphi\dot{\delta} - m_f l_f g(\theta + \varepsilon) \end{bmatrix}. \tag{16}$$

[2] The notation c_α and s_α, with $\alpha \in \mathbb{R}$, stands for $\cos\alpha$ and $\sin\alpha$, respectively.

Finally, note that, given the nonlinear model σ in (15), and considering the (passive) control force defined in equation (8)), we can compute the total absorbed mechanical power P_a, for a given time interval $\Xi = [0,\, T] \subset \mathbb{R}^+$, as

$$P_a = \frac{1}{T}\int_{\Xi} c_{\text{PTO}}\dot{\varepsilon}(t)^2 \mathrm{d}t = \frac{1}{T}\int_{\Xi} P_i(t)\mathrm{d}t, \qquad (17)$$

where T corresponds to the wave period, and $P_i = c_{\text{PTO}}\dot{\varepsilon}^2$ is the associated instantaneous mechanical power.

2.5 Harmonic Balance approach

Harmonic balance (HB) is an extensively used technique for dynamic analysis of nonlinear systems, especially those inherently involving periodic motions such as the SWINGO device. It is based upon an approximation of the system variables in the form of a truncated Fourier series. In this section, we introduce the main steps for the HB implementation applied in this paper, which are based upon the theory presented in *e.g.* (Giorgi and Faedo, 2022).

We begin by noting that equation (15) can be re-written in terms of a continuous-time, state-space, system, defining the dynamics of the SWINGO device such that

$$\sigma : \{\ \dot{\pi} = f(\pi, f_{ex}), \qquad (18)$$

where $\pi(t) = [\rho(t)^\intercal\ \dot{\rho}(t)^\intercal]^\intercal \in \mathbb{R}^n$, with the variable $\rho(t) = [\gamma(t)^\intercal\ \varepsilon(t)]^\intercal \in \mathbb{R}^3$ and, hence, $n = 6$, denotes the state-vector of (18), $f_{ex}(t) = T_w(t) \in \mathbb{R}^2$ represents the forcing term, and $f : \mathbb{R}^n \times \mathbb{R}^2 \to \mathbb{R}^n$ is the corresponding state-transition map (which can be straightforwardly derived from (15)). As per standard HB theory, we assume that the (steady-state) solution of (18) can be approximated in terms of a finite-dimensional space $\mathscr{H} = \text{span}(\mathscr{X})$, with

$$\mathscr{X} = \{c_{p\omega t}, s_{p\omega t}\}_{p=1}^{N}, \qquad (19)$$

where the set $\mathscr{X}$ is complete, and $\mathscr{H} \subset L^2(\Omega)$, with $\Omega = [0, T] \subset \mathbb{R}^+$. In this particular study, we consider an ansatz with only a single harmonic, *i.e.* $N = 1$ in (19). To be precise, $\pi_i \approx \tilde{\pi}_i$, where $\tilde{\pi}_i \in \mathscr{H}$, can be expressed as follows

$$\tilde{\pi}_i(t) = \alpha_i c_{\omega t} + \beta_i s_{\omega t},\ T = \frac{2\pi}{\omega}, \qquad (20)$$

with $i \in \mathbb{N}_n$, and $\{\alpha_i, \beta_i\} \subset \mathbb{R}$. We note that ω is called herein fundamental harmonic. The approximation $\tilde{\pi}$ of the full state-vector can be written as

$$\tilde{\pi}(t) = \left[\tilde{\Pi}_1^\intercal\ \ldots\ \tilde{\Pi}_n^\intercal\right]^\intercal \Theta(t) = \tilde{\Pi}\Theta(t), \qquad (21)$$

where $\{\tilde{\Pi}_i^\intercal, \Theta(t)\} \subset \mathbb{R}^2$, $\forall i \in \mathbb{N}_n$, are defined such that $\tilde{\Pi}_i = [\alpha_i\ \beta_i]$ and $\Theta(t) = [c_{\omega t}\ s_{\omega t}]^\intercal$. The forcing function f_{ex} can be expressed as a function of Θ through an appropriate inclusion map, *i.e.*

$$f_{ex}(t) = F_{ex}c_{\omega t} + F_{ey}s_{\omega t} = \tilde{F}\Theta(t), \qquad (22)$$

where $\tilde{F} = [F_{ex}\, F_{ey}]$. We define the residual function $\mathscr{R}$ as

$$\mathscr{R}(\tilde{\Pi}, \tilde{F}, \Theta) \equiv \dot{\tilde{\pi}} - f(\tilde{\pi}, f_{ex}) = \tilde{\Pi}\dot{\Theta} - f(\tilde{\Pi}\Theta, \tilde{F}\Theta), \qquad (23)$$

and let $\mathscr{D}_c = \{\mu(t - t_j) = \mu_j\}_{j=1}^{q} \subset \Omega$, with $q > nN$, be a set of shifted generalised Dirac-delta functions. Finally, using the standard inner product in $L^2(\Omega)$, the expansion coefficients $\tilde{\Pi}$, defining the approximating solution $\tilde{\pi}$, can be computed via a Galerkin (pseudospectral) approach, where the projection of the residual function (23) onto the set $\mathscr{D}_c$ is forced to be zero for $j \in \mathbb{N}_q$, *i.e.*

$$\langle \mathscr{R}, \mu_j \rangle = 0. \qquad (24)$$

3. PASSIVE CONTROL DESIGN

In this section, we introduce the dynamical characterisation of the SWINGO, excited by regular waves, through the solution of the equation expressed in (15). Then, via a HB procedure (see Section 2.5), we aim a) to assess the dynamical properties of the WEC described equation (15) (alternatively equation (16)), and b) compute the optimal passive control parameter in equation (8) taking into account the system stability.

Moreover, making explicit use of the corresponding AFC for the subsequent analysis, we can now provide a definition of amplitude as a function of the input frequency as follows: Given an excitation input f_{ex} with frequency ω and amplitude $\tilde{F}$ (as in (22)), and the corresponding HB solution, we define the associated set of amplitudes for the set of variables $\{\tilde{\varepsilon}, \dot{\tilde{\varepsilon}}\} \subset \mathbb{R}^+$ as

$$\tilde{\varepsilon} = \sqrt{\alpha_3^2 + \beta_3^2}, \qquad \dot{\tilde{\varepsilon}} = \sqrt{\alpha_6^2 + \beta_6^2}. \qquad (25)$$

Based on such a definition, Figure 2 shows the SWINGO performance in terms of both $\varepsilon_0 = \tilde{\varepsilon}/\varepsilon_{cons}$, where ε_{cons} is the constraint value related to the gyropendulm rotation due to physical limitations of the device components, and scaled power. The latter is defined by the ratio between the mean power and maximum power $P_{a_{max}}$ derived from the nonlinear model. Such performance indexes are evaluated through the AFC as a function of $\bar{c} = c_{\text{PTO}}/c_{opt}$, where c_{opt} is the damping parameter corresponding with the condition of maximum power transfer derived with the nonlinear model in equation (15). We recall that, analogously

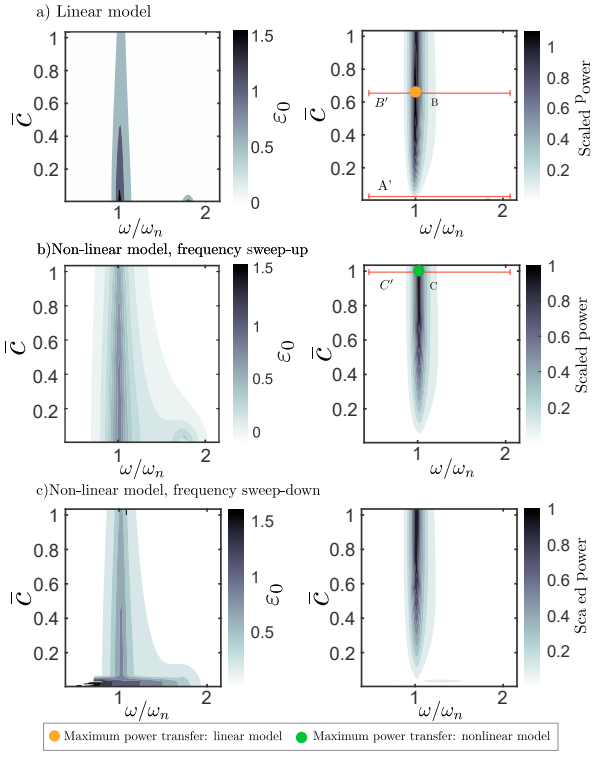

Fig. 2. Contour plot of the scaled rotation ε_0 (left) and scaled power (right) as a function of ω/ω_h and $\bar{c}$.

to (Carapellese et al., 2022a), the AFCs plots presented in Figure 2 are computed based upon both a sweep-up and sweep-down frequency-dependent procedure. In the case

of the former, HB is initiated from the lowest frequency component considered, and its associated solution is used as a starting point for the following (up) frequency, until the highest frequency value studied is reached. The latter is performed analogously, but in the opposite sense. Note that the amplitude of the input signal, which effectively depends upon the chosen frequency ω, is computed in terms of the so-called excitation force kernel (see *e.g.* (Falnes, 2002)), taking into consideration a unitary free-surface elevation. In particular all the frequency plots introduce the frequency ratio ω/ω_h, where ω_h is the hydrodynamic resonance of the system (e.g. see (Carapellese et al., 2022b)). We note that both models present the optimality power absorption condition at resonance, i.e. $\omega/\omega_h = 1$, although the optimal passive control parameters, denoted with green and orange dots in the plot for the nonlinear and linear models, are effectively different. The linear model overestimates the gyropendulum motion, having an impact on the extracted power, and on the control parameter selection. Then, the optimal damping c_{opt} computed from the nonlinear model is about 30% larger than the parameter designed from its linear counterpart. A deeper

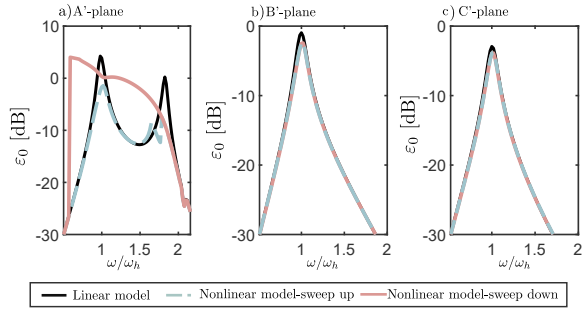

Fig. 3. AFC referred to the damping values corresponding with points A', B', and C' in Figure 2.

analysis is performed in Figure 3, where an appraisal of the AFCs corresponding to the zero control condition (see Figure 2 AFC **A'**), and the optimal damping condition derived both via linear and nonlinear model (AFC **B'** and **C'**) are represented. We note that for a value of $\bar{c} = 0$, two different solutions co-exist for the considered input signal, depending on the initial condition of the system (15). Such a bistability effect persists up to the value of $\bar{c} = 0.2$, a condition where the nonlinear model converges to a unique solution, independently from the HB sweep direction. Therefore, for higher values of $\bar{c}$, approaching both **B'** and **C'**, the behaviour of the nonlinear model resembles a linear behaviour, since the damping effectively ameliorates the main nonlinear effects. Nonetheless, the motion resulting from the linear model, computed via Jacobian linearisation, overestimate the response arising from the nonlinear model in equation (15).

Even if the sweep bidirectionality approach is a widely used numerical method for the definition of the AFC of a nonlinear system, it does not necessarily capture all the relevant system solutions. In the light of this, an exhaustive search of potential SWINGO system solutions is performed at resonance, *i.e.* when $\omega/\omega_h = 1$, through the HB procedure. The stability plot in Figure 4 introduces the normalised gyropendulum kinematics variable $\tilde{\varepsilon}_n$ and $\dot{\tilde{\varepsilon}}_n$, as a function of $\bar{c}$. The plot clearly shows three different

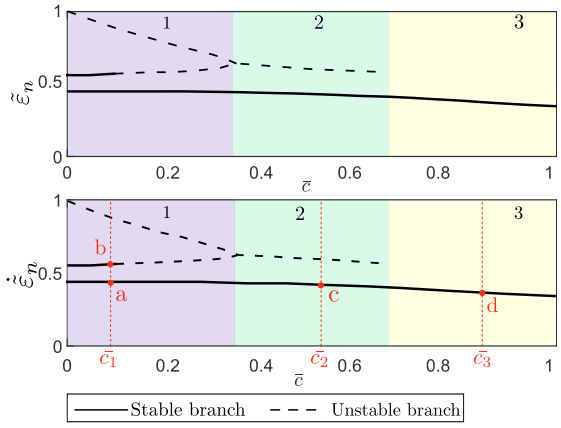

Fig. 4. Stability diagram of the solution $\tilde{\varepsilon}_n$ and $\dot{\tilde{\varepsilon}}_n$ as a function of $\bar{c}$, for ω/ω_h=1.

solution 'zones', where the number of system solutions range from three in zone 1 (for a low value of $\bar{c}$), to zone 3, where one solution exists. The stability of every solution presented in Figure 4 is addressed in detail in Section (4).

4. STABILITY ANALYSIS

We consider, within this section, the so-called van der Pol plane (see (Jordan and Smith, 2007)) to discuss the stability of the solutions of (15), corresponding to the set of damping values $\{\bar{c}_1, \bar{c}_2, \bar{c}_3\}$, as defined in Figure 4.

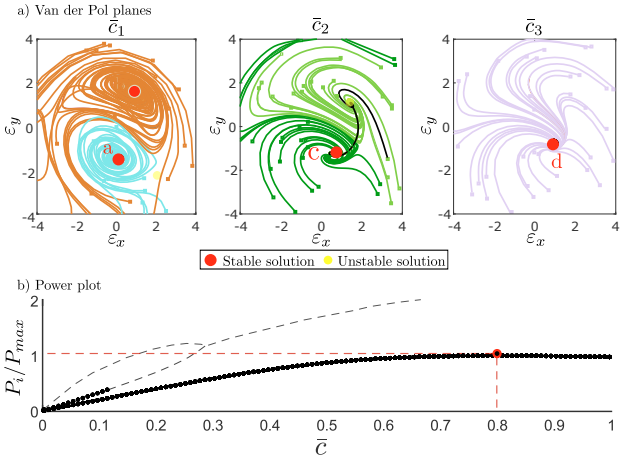

Fig. 5. Van der Pol plane referred to the three different control conditions: $\bar{c}_1$, $\bar{c}_2$ and $\bar{c}_3$ (a). Normalised mean power as a function of $\bar{c}$ (b).

In particular, to investigate the stability of the different solutions, we analyse the 'transient states', by using different initial conditions for the system under study. The associated 'paths' can either converge to a stable periodic orbit, or generate an unstable solution. For these purposes, and in line with the HB theory previously considered, we assume that the coefficients α_i and β_i in equation (20) are slowly varying functions of time, at any rate near to periodic solution. Assuming that at least one stable solution exists, we apply the underlying concept of the van der Pol diagram to study the stability properties of the solution presented in Figure 4, defining the region of attraction related to each solution. For the SWINGO device, we recognise that the manifold, describing the evolution of the

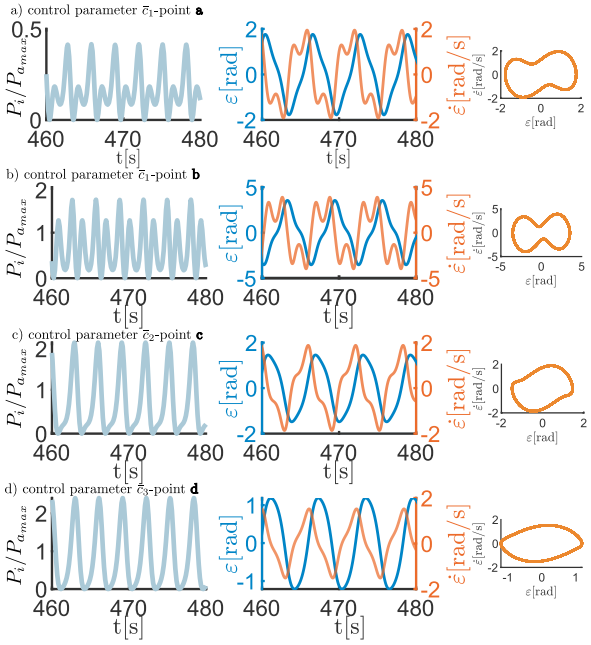

Fig. 6. Time series of the instantaneous power (left), gyropendulum kinematics (ε and $\dot{\varepsilon}$ in the middle) and phase diagrams (right) for different control conditions.

system, generates a multidimensional problem. Nevertheless, we do present in this paper a planar projection of the system evolution focusing of the gyropendulum oscillation, *i.e.* we assume

$$\hat{\varepsilon}(t) = \varepsilon_x(t)c_{\omega_h t} + \varepsilon_y(t)s_{\omega_h t}, \tag{26}$$

where $\hat{\varepsilon}(t) \in \mathbb{R}$ is the approximation of the state ε, as a function of the slowly varying amplitudes ε_x and ε_y. The phase plane for $(\varepsilon_x, \varepsilon_y)$ is called the van der Pol plane. We show, from Figure 5, that solutions **a** and **b** are stable, since they correspond to two different areas of attraction, depending on the initial condition (highligthed in the plot with square markers). The yellow dot in Figure 5 marks the third solution within zone 1 (see Figure 4) corresponding to an unstable solution. When in the $\bar{c}_2$ condition, the system presents only one stable solution converging to the point **c**. Note that, in Figure 5, the paths that, even if vortexing with respect to the yellow dot, they do still converge to the attractor **c**, are shown with light-green lines. To further clarify this, Figure 5 highlights one particular path by using a solid black line, which can be clearly seen to converge to the **c** solution. Finally, for high values of $\bar{c}$, the system exhibits only one stable solution **d**.

From this analysis, we can determine the stable branches corresponding with the gyropendulum kinematic parameters introduced in Figure 4, and hence derive the power plot shown in Figure 5. We prove that, although multiple solutions are present, the optimal physically achievable maximum mean power value $P_{a_{max}}$ happens for a value of $\bar{c}$ falling in zone 3, where a single solution exists. Figure 6 represents the time series of the instantaneous power P_i normalised with respect to $P_{a_{max}}$, and the gyropendulum kinematic time series corresponding to each stable system solution. We can appreciate the time traces and the phase plot of the solution **a** and **b**, which correspond to the same simulation condition, illustrating the bistability effect of SWINGO small values of $\bar{c}$.

5. CONCLUSION

From the nonlinear model of the SWINGO device with respect to quasi-coordinates, we present, in this paper, a dynamic analysis of the system, correlated with the design of the passive control parameter that guarantees the condition of maximum power transfer. All the analysis are performed using the HB procedure, explicitly showing that linear and nonlinear models present significant differences, which have an impact on control synthesis and performance assessment. Moreover, even if the system presents a bistability behaviour for specific conditions, through the van der Pol plane, we demonstrate that, in the optimality condition, the system has a single point of attraction.

REFERENCES

Carapellese, F., Pasta, E., Faedo, N., and Giorgi, G. (2022a). Dynamic analysis and performance assessment of the Inertial Sea Wave Energy Converter (ISWEC) device via harmonic balance. In *14th IFAC Conference on Control Applications in Marine Systems, Robotics and Vehicles*. Lyngby, Denmark.

Carapellese, F., Pasta, E., Paduano, B., Faedo, N., and Mattiazzo, G. (2022b). Intuitive LTI energy-maximising control for multi-degree of freedom wave energy converters: The PeWEC case. *Ocean Engineering*, 256, 111444. doi:10.1016/j.oceaneng.2022.111444.

Carapellese, F., Pasta, E., Sirigu, A.S., and Faedo, N. (2023). SWINGO: Conceptualization, modelling and control of a swinging omni-directional Wave Energy Converter. *Mechanical Systems and Signal Processing*.

Falnes, J. (2002). *Ocean Waves and Oscillating Systems*. Cambridge University Press. doi: 10.1017/CBO9780511754630.

Genta, G. (2009). *Vibration Dynamics and Control*. Mechanical Engineering Series. Springer US, Boston, MA. doi:10.1007/978-0-387-79580-5.

Gioia, D.G., Pasta, E., Brandimarte, P., and Mattiazzo, G. (2022). Data-driven control of a Pendulum Wave Energy Converter: A Gaussian Process Regression approach. *Ocean Engineering*, 253, 111191. doi: 10.1016/j.oceaneng.2022.111191.

Giorgi, G. and Faedo, N. (2022). Performance enhancement of a vibration energy harvester via harmonic time-varying damping: A pseudospectral-based approach. *Mechanical Systems and Signal Processing*, 165, 108331. doi:10.1016/j.ymssp.2021.108331.

Gunn, K. and Stock-Williams, C. (2012). Quantifying the global wave power resource. *Renewable Energy*, 44, 296–304. doi:10.1016/j.renene.2012.01.101.

Jordan, D.W. and Smith, P. (2007). *Nonlinear Ordinary Differential Equations: an introduction for scientists and engineers*. Oxford University Press.

Meirovitch, L. (1970). *Methods of analytical dynamics*. McGraw-Hill.

Siciliano, B., Sciavicco, L., Villani, L., and Oriolo, G. (2009). *Robotics: Modeling, Planning, and Control*. Springer.

Windt, C., Faedo, N., Penalba, M., Dias, F., and Ringwood, J.V. (2021). Reactive control of wave energy devices – the modelling paradox. *Applied Ocean Research*, 109, 102574. doi:10.1016/j.apor.2021.102574.